An Analytical and Numerical Sensitivity and Robustness Analysis of Wave Energy Control Systems

An Analytical and Numerical Sensitivity and Robustness Analysis of Wave Energy Control Systems

John V. Ringwood, *Senior Member, IEEE*, Alexis Mérigaud, Nicolás Faedo, and Francesco Fusco

***Abstract*— Considerable effort has been expended on the design of control systems for wave energy converters (WECs) over the past two decades. Working from the fundamental requirement of impedance matching, a variety of conceptual and practical algorithms have emerged, which bring various levels of realism to the original complex conjugate ideal, facilitating maximum power transfer. Simplifications can be introduced, such as passive control and causal control, while some enhanced algorithms allow physical constraints to be observed, nonlinear model dynamics to be articulated, or nonideal power takeoff systems to be recognized. However, in general, model-based WEC control systems are evaluated in tandem with identical simulation models, while the sensitivity of controller performance to modeling errors is ignored. In addition, the WEC model utilized by the controller rarely, if ever, fully represents the nonlinear nature of the true WEC dynamics. This paper articulates this model sensitivity issue for different WEC control system architectures and shows that it is of potentially greater impact than for traditional regulation/servomechanism control problems. Recommendations are given on the best WEC control architecture to adopt from a sensitivity/robustness perspective.**

***Index Terms*— Control system, robustness, sensitivity, wave energy.**

I. Introduction

AS PART of the challenge of bringing wave energy to economic viability, control systems are seen as a key enabler to maximize energy capture for a given capital cost of the wave energy converter (WECs) devices [1]. Methods to enhance the energy capture capabilities of WECs have been reported since 1970's [2] and many varieties of WEC control methodology have been reported in the interim, including latching/declutching control [3] and model-predictive control (MPC) [4], as well as a variety of other techniques [5]. The vast majority of these control strategies is model-based and relies on a hydrodynamic model, which describes the mathematical relationship between the incident waves and the mechanical response of the WEC. Note that, in this paper, we focus solely on hydrodynamic control aspects, while a fuller treatment would also consider aspects of the power takeoff (PTO) system [6], which converts the mechanical energy to a more useable form, such as electrical energy.

One particular property of WEC control systems, which has received little attention to date, is the degree to which the model-based WEC control strategies are *sensitive* to WEC modeling errors, i.e., how *robust* are model-based WEC control systems? There are a variety of reasons why modeling errors are present, and potentially significant, in current model-based WEC control strategies.

1) Linear hydrodynamic theory is well established and, given the considerable difficulty attached to the calculation of *linear* hydrodynamic parameters, there is little appetite to extend these models to include nonlinear effects.
2) The assumptions under which the linearization of WEC models is performed are challenged, particularly in relation to small movements around the equilibrium position (in fact, the control objective is to exaggerate motion).
3) Model-based control strategies must run in real time, therefore limiting the computational complexity of the hydrodynamic models employed (for example, high-fidelity hydrodynamic models based on computational fluid dynamics (CFD) typically run in approximately 1000× real time).
4) There is a limit to the complexity of hydrodynamic models for which an optimal control solution can be found either algebraically or numerically.
5) Many WEC hydrodynamic models are evaluated/validated in tank tests where the excitation is provided only through the variation in the free-surface elevation with no external PTO force present (this issue will be explored further in Section II-A).
6) WEC controllers are often validated in simulation using the exact model upon which the controller was determined, thus masking any sensitivity issues.

It is well known that the closed-loop sensitivity of traditional servo/regulatory control loops is enhanced through feedback control (and can be further enhanced through dedicated robust

Manuscript received June 28, 2018; accepted March 29, 2019. Manuscript received in final form April 1, 2019. This work was supported by Science Foundation Ireland through the Marine Renewable Ireland (MaREI) Centre under Grant SFI/13/IA/1886 and Grant 12/RC/2302. Recommended by Associate Editor H. R. Pota. *(Corresponding author: John V. Ringwood.)*

J. V. Ringwood and N. Faedo are with the Centre for Ocean Energy Research, Maynooth University, Maynooth, Ireland (e-mail: john.ringwood@mu.ie; nicolas.faedo.2017@mumail.ie).

A. Mérigaud is with IFP Energies Nouvelles, 92852 Rueil-Malmaison, France (e-mail: alexis.merigaud@ifpen.fr).

F. Fusco is with Smarter Cities Technology, IBM Research—Ireland, Dublin 15, Ireland (e-mail: francfus@ie.ibm.com).

Color versions of one or more of the figures in this paper are available online at http://ieeexplore.ieee.org.

Digital Object Identifier 10.1109/TCST.2019.2909719

control synthesis [7]). However, this is not necessarily the case for energy maximizing control systems, since many WEC controllers contain a feedforward part, and the energy maximizing control objective leads to a very specific relationship between controller and plant, preventing the traditional use of high gain to reduce sensitivity. While a number of studies have examined the robustness of specific WEC controllers [8], [9], and some attempts have been made to synthesize WEC controllers that are robust to particular parametric variation [10], [11], to date there has been no generic study of WEC controller sensitivity and robustness properties to highlight the issues and provide some guidance on model accuracy requirements. This paper aims to fill that gap.

In this paper, the focus is on linear hydrodynamic models, which provide an initial platform for analysis while, to a certain extent, nonlinear modeling errors can be represented by variations in linear system dynamics. The reason for this is twofold. First, we wish to employ the WEC model that is prevalent in the literature (and in practice) and, second, using a linear model with perturbation is well established as a foundation for robust control [12], where the perturbation can represent variation in the linear model due to uncertainty or modeling error, nonlinearity, or time-varying behavior. This paper examines the sensitivity of model-based WEC control schemes from three points of view.

1) Various components, comprising a linear hydrodynamic model, are examined with reference to the importance of their relative fidelity in an energy maximizing control strategy.
2) The sensitivity function, which is straightforwardly calculated for traditional servo/regulator control loops, is evaluated for WEC control system structures.
3) The sensitivity of the converted power in the WEC is calculated with respect to typical modeling errors contained within model-based WEC control strategies.

The analysis, covering the three perspectives described above, is detailed for two popular WEC control architectures, allowing some conclusions to be drawn regarding the optimal WEC control architecture from a sensitivity/robustness perspective. Note that this paper does not specifically address robust controller synthesis per se, but rather focusses on generic sensitivity analysis, to provide a comprehensive platform for future efforts in robust WEC controller synthesis.

The remainder of this paper is organized as follows. Section II articulates the standard WEC modeling paradigms and assumptions, combined with a description of typical WEC controller structures. The main body of analysis is contained in Sections III and IV, which examine the sensitivity of the closed-loop systems, and power production, respectively, to the variations in model parameters for different control structures considered. In general, the results of Sections III and IV focus on generic (predominantly frequency domain) properties, illustrated with some examples, whereas Section V presents the sample time-domain simulation results. Conclusions, with a specific focus on recommendations for WEC modeling, based on the results achieved in this paper, are presented in Section VI.

II. WEC Models and Controllers

A. WEC Models for Model-Based Control

Consider a single-body floating system oscillating in heave, schematically depicted in Fig. 1. Energy is extracted from the relative motion with the sea bottom through a generic PTO mechanism.

Neglecting mooring forces, the external forces acting on the WEC are the gravity force, the hydrodynamic and hydrostatic forces resulting from the interaction of the WEC with the surrounding fluid, and the control force f_{PTO} produced by the PTO.

With the assumptions associated with linear potential theory [13] (namely, that the fluid is irrotational, incompressible, and inviscid) and assuming that the body experiences small oscillations, the hydrodynamic and hydrostatic forces acting on the WEC body can be separated into three components in the following.

1) The buoyancy (or hydrostatic) force, f_b, is related to the deflection of the device from its equilibrium (still water) position and is a balance between the Archimedes buoyancy force and the gravity force [13].
2) The excitation force, f_{ex}, represents the integral of the pressure forces due to the incident waves acting on the body. f_{ex} depends on the incident waves and on the position and geometry of the body. It can be thought of as the force required to maintain the body still in the presence of incident waves.
3) The radiation force, f_r, is a damping/inertial force associated with the device motion caused by the production of radiated waves. Such radiation forces are present even in the absence of incident waves and can be estimated using free-response tests.

Therefore, the equation of motion, in one degree of freedom, following Newton's second law, is given as:

$$M\dot{v}(t) = f_{\text{ex}}(t) + f_r(t) + f_b(t) + f_{\text{PTO}}(t) \tag{1}$$

where $v(t)$ is the heaving velocity and M is the WEC mass.

Assuming that the WEC body has a small cross-sectional area (or equivalently, that the wave elevation is constant across the whole body), the hydrodynamic and hydrostatic terms in (1) can be expressed as

$$f_{\text{ex}}(t) = \int_{-\infty}^{+\infty} h_{\text{ex}}(\tau)\eta(t-\tau)d\tau \tag{2}$$

$$f_r(t) = -\int_0^t h_r(\tau)v(t-\tau)d\tau - m_\infty \dot{v}(t) \tag{3}$$

$$f_b(t) = -\rho g S_w \int_0^t v(\tau)d\tau = -kx(t) \tag{4}$$

where $x(t)$ is the device (heave) displacement and $h_{\text{ex}}(t)$ and $h_r(t)$ represent the impulse response kernels relating to the excitation force and radiation damping, respectively. $\eta(t)$ is the variation in the free-surface elevation with time. The buoyancy force $f_b(t)$ models the hydrostatic equilibrium, related to the heaving position through a linear coefficient that depends on the gravity acceleration g, the water density ρ, and the surface area of the body cut by the mean water level S_w. Note that the

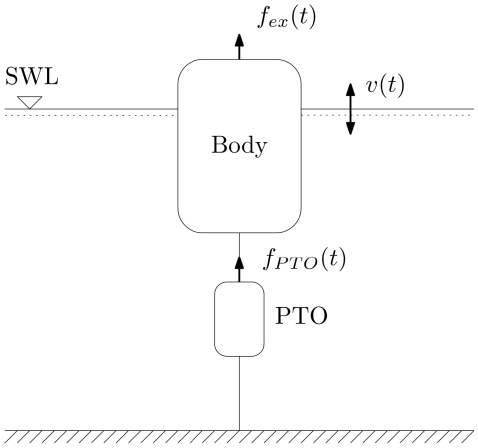

Fig. 1. One degree-of-freedom floating system for wave-energy conversion. The bottom side of the PTO is anchored to the sea bed, which provides an absolute reference for device motion. SWL: still water level.

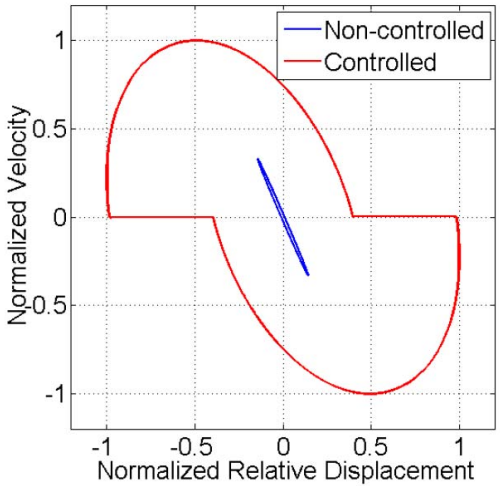

Fig. 2. Operational space covered by uncontrolled and controlled spherical heaving buoys.

noncausality of the expression for the excitation force, where $h_{\text{ex}}(t) \neq 0$ for $t \leq 0$ [13]. Equation (1) results in the widely used Cummins' equation [14]

$$(M + m_\infty)\dot{v}(t) + \int_0^{+\infty} h_r(\tau)v(t-\tau)d\tau + kx(t) = \int_{-\infty}^{+\infty} h_{\text{ex}}(\tau)\eta(t-\tau)d\tau + f_{\text{PTO}}(t). \quad (5)$$

The model in (5), widespread in WEC control studies, has the following limitations.

1) There is an assumption that the device experiences small oscillations, while the objective, in maximum energy capture, is to exaggerate motion.
2) Viscous effects are ignored. The viscous damping force is a nonlinear force and becomes significant with the increased device velocity [15]. It is particularly relevant where the body surface contains discontinuities (such as flanges), which result in the creation of vortices.
3) Linear excitation and buoyancy forces are only reasonable when the oscillating body has a uniform cross-sectional area [15].
4) For the purposes of control design, the nonparametric descriptions of $h_r(t)$ and $h_{\text{ex}}(t)$ in (5) are normally approximated using finite order representations, for example, using the techniques described in [16] or [17].

In addition, WEC models, determined under uncontrolled conditions, are probably not representative, with Fig. 2 showing the operational space (in terms of velocity and displacement) covered by an uncontrolled, and a (latching) controlled, spherical heaving buoy [18]. Under controlled conditions, there are increases in viscous effects (due to relative device/fluid velocity) and nonlinear Froude-Krylov (excitation/buoyancy) forces (due to increases in the wetted surface variation).

Finally, there are also likely to be minor inaccuracies in the determination of $h_r(\tau)$ and m_∞ via mesh-based linear boundary element solvers, due to discretization of the domain, and other effects. Overall, then, there is likely to be a significant disparity between the real WEC dynamics and those represented in (5), typically used for the model-based controller development. However, these system/controller mismatch issues are frequently masked by the employment of a simulation/evaluation model that is also based on (5), which tends to be relatively common practice in WEC control studies.

B. WEC Control Structures

WEC controllers are employed to maximize converted wave power. A preliminary analysis can be carried out by considering the frequency-domain equivalent of (5), namely,

$$\frac{V(\omega)}{F_{\text{ex}}(\omega) + F_{\text{PTO}}(\omega)} = \frac{1}{Z_i(\omega)} \quad (6)$$

where $W(\omega) = \mathcal{F}\{w(t)\}$ the Fourier transform of $w(t)$. The intrinsic WEC impedance $Z_i(\omega)$ is

$$Z_i(\omega) = B_r(\omega) + \jmath\omega\left[M + M_a(\omega) - \frac{k}{\omega^2}\right] \quad (7)$$

where m_∞ in (5) is the infinite frequency asymptote of the added mass $M_a(\omega)$, and we note that, for radiation damping

$$\mathcal{F}\{h_r(t)\} = B_r(\omega) + j\omega[M_a(\omega) - m_\infty] \quad (8)$$

relating $h_r(t)$ in (5) to B_r in (7). For the maximum power transfer, we choose a controller "impedance" $Z_c(\omega)$ so that

$$Z_c(\omega) = Z_i^*(\omega) \quad (9)$$

where z^* denotes the complex conjugate of $z \in \mathbb{C}$. Alternatively, an optimal velocity profile $V_{\text{opt}}(\omega)$ to follow can be generated [13] as

$$V_{\text{opt}}(\omega) = \frac{F_{\text{ex}}(\omega)}{2R_i(\omega)} \quad (10)$$

where $R_i = B_r(\omega) = 1/2\ (Z_i + Z_i^*)$ is the real part of Z_i. Equations (9) and (10) essentially lead to the two fundamental WEC controller configurations: 1) the approximate complex-conjugate control (ACC) structure and 2) the approximate optimal velocity tracking (AVT) structure, following the designation of Hals *et al.* [19]. The ACC controller, which directly

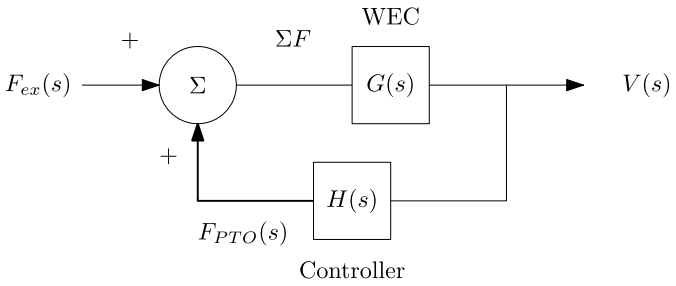

Fig. 3. ACC controller structure, which directly calculates the PTO force, using (9).

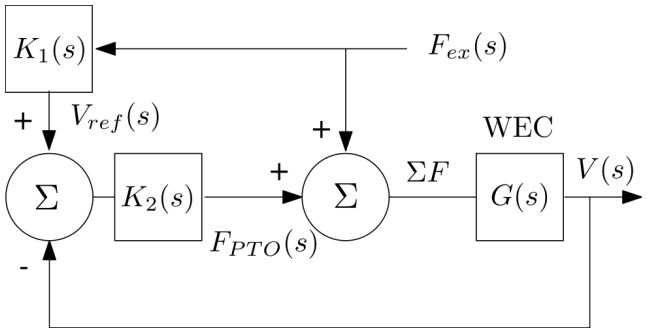

Fig. 4. AVT controller structure, which calculates the optimal velocity profile, prior to the use of a tracking control loop to achieve that velocity profile.

produces a PTO force input from measurement of device velocity, is shown in Fig. 3, whereas the AVT controller, which first calculates the optimal velocity trajectory, and subsequently implements a tracking control loop to follow that trajectory, is shown in Fig. 4.

The various components of the ACC and AVT controllers are defined, in the Laplace domain, as follows:

- $G(s)$ is the linear WEC model, which defines the velocity $V(s)$ resulting from the application of a combination of excitation force $F_{\text{ex}}(s)$ and PTO force $F_{\text{PTO}}(s)$;
- $H(s)$ is the direct force WEC controller;
- $K_1(s)$ is the velocity setpoint calculation, based on the excitation force F_{ex};
- $K_2(s)$ is the feedback controller that tries to maintain the WEC velocity profile at its setpoint.

We note that $G(s)$ contains a finite-order linear dynamic approximation to the nonparametric impulse response excitation force and radiation damping kernels that typically result from the hydrodynamic parameters calculated using boundary-element methods, such as WAMIT [20].

In the ACC controller, the control force can be suitably parameterized as

$$f_{\text{PTO}}(t) = M_c\ddot{x}(t) + B_c\dot{x}(t) + k_c x(t) \tag{11}$$

giving

$$Z_c = B_c + j\left(\omega M_c - \frac{k_c}{\omega}\right) \tag{12}$$

and $H(s)$ represents the Laplace equivalent of $Z_c(\omega)$.

Three controller parameter set (M_c, B_c, and K_c) choices all achieve the required complex conjugate [21]

$$M_c(\omega) = -(M + M_a(\omega)) + \frac{k}{\omega^2}, \quad k_c = 0, \quad B_c = B_r \tag{13}$$

$$k_c(\omega) = (M + M_a(\omega))\,\omega^2 - k, \quad M_c = 0, \quad B_c = B_r \tag{14}$$

$$M_c(\omega) = -(M + M_a(\omega)), \quad k_c = -k, \quad B_c = B_r. \tag{15}$$

We can note that the three-term controller (11) has, effectively, one redundant term, since only a combination that yields a single real and imaginary term [i.e., (13) and (14)] is required to achieve the condition in (9), with Hansen [21] suggesting that (14) is preferred.

For the AVT case, the controller is not so easily parameterized but uses a direct implementation of (10). Some notes on these basic controller configurations are appropriate at this point.

1) Both (9) and (10) are the functions of frequency ω, indicating that either only a single wave frequency is handled or that the controller parameters must be adapted with frequency. In practice, a panchromatic version of the ACC controller has been developed [22], while $v_{\text{ref}}(t)$, in the AVT controller, is usually evaluated as the solution of a numerical optimization problem [23].
2) One critical aspect, common to many control applications, is the need to keep key system variables (displacement, velocity, and force) within physical limits. While the basic calculations in (9) and (10) pay no heed to physical constraints, constrained optimization can be used [23] to ensure physical constraints are obeyed. In general, constrained solutions for the ACC controller are not yet available.
3) Since $h_r(t)$ is causal, $h_c(t) = \mathcal{F}^{-1}\{Z_c(\omega)\}$ (inverse Fourier transform of Z_c) is anticausal, requiring future knowledge of the excitation force. While this knowledge is straightforward for the monochromatic case (single sinusoid), it is more problematic for irregular seas. The issue of forecasting random seas is dealt with in [24] and [25]. We note that, since it is based on instantaneous velocity feedback, the simpler ACC controller has the advantage that it does not require future values of the excitation force. However, a suboptimal causal solution is required, for the panchromatic case, as a result [22].

The issues outlined above significantly complicate any robustness/sensitivity analysis. As a consequence, where possible, we will assume perfect future knowledge of f_{ex}, though some consideration of errors in f_{ex} will be given in Section III, while a more thorough treatment of the effects of f_{ex} forecast errors is given in [26]. For the present, physical constraints will be addressed in a somewhat qualitative way.

C. Control Dependencies

Before studying the sensitivity of WEC energy maximizing control to modeling errors, it is worth noting that optimal control results exhibit varying dependencies on different types of forces and constraints in the control calculations.

As shown in [22] and [27], neither the unconstrained optimal velocity trajectory nor the optimal power is influenced by the linear inertial terms, and nor by linear or nonlinear static forces, i.e., forces that solely depend on the WEC position. This result remains true under position and velocity constraints but not under constraints involving the control force (e.g., PTO force constraints, or limitations on the instantaneous power) [27]. In contrast, the required control force *always* depends on all the model dynamics (inertial, velocity dependent, and static terms). Therefore:

1) In unconstrained conditions or under position and velocity constraints, the upper loop of the AVT controller is insensitive to modeling errors on inertial and static terms. Although the optimal PTO force, necessary to achieve the optimal trajectory, is not independent of inertial and static terms, any sensitivity to those modeling errors can be mitigated via the classical feedback effect of the velocity tracking loop of the AVT control structure.
2) This sensitivity reduction is not possible for the ACC structure, as will be demonstrated in Section III-A, since all the device dynamics are involved in the optimal control law (11).

Velocity-dependent forces always influence the optimal velocity trajectory, control force, and power output, regardless of the presence/absence of constraints [27]. In the unconstrained case, or under position and velocity limitations, velocity-dependent forces are the only terms, in addition to excitation forces, which govern the optimal trajectory. As a consequence, it must be ensured that in the following.

1) Radiation damping is well modeled; in particular, any approximation to the radiation damping convolution integral must have good fidelity.
2) Any viscous drag or other velocity-dependent losses are appropriately modeled.

The sensitivity of power absorption to modeling errors in inertial, velocity dependent, and static terms will be studied in more detail in Section IV.

III. Closed-Loop Transfer Function Sensitivity

From the wealth of knowledge concerning classical tracking feedback systems, one might expect the ACC feedback structure (Fig. 3) to have good sensitivity properties, whereas the feedforward calculation involved in the K_1 block of the AVT controller (Fig. 4) might be expected to be more sensitive. However, the design of $H(s)$ in the ACC controller, which must ensure maximum power transfer, severely limits any freedom to manipulate the system sensitivity. Nevertheless, the feedback loop in the AVT controller is a standard tracking loop, so standard robustness techniques can be applied [10].

In this section, we determine the sensitivity of the overall closed-loop transfer function (CLTF), $T(s) = V(s)/F_{\text{ex}}(s)$, to the variations in the WEC model, $G(s)$. Note that the example analytical calculations of Sections III and IV utilize a cylindrical WEC with a 7 [m] radius, 20 [m] height, and 16 [m] draft, consistent with the device used for the simulation studies in Section V, where it is described in more detail, along with the incident wave conditions used.

A. ACC Structure

In the following, the nominal transfer function for the frequency response model (12) of the ACC controller is expressed via its Laplace domain counterpart, assuming that $s \in \mathbb{C}^0$, where $\mathbb{C}^0$ denotes the set of pure imaginary complex numbers. The transfer functions of the WEC device $G(s)$, and the complex conjugate controller $H(s)$, in Fig. 3, are given, respectively, by

$$G(s) = \frac{s}{(M + M_a^\omega)s^2 + B_r^\omega s + k} \tag{16}$$

$$H(s) = \frac{-(M + M_a^\omega)s^2 + B_r^\omega s - k}{s} \tag{17}$$

where $B_r^\omega = B_r(\omega)$ and $M_a^\omega = M_a(\omega)$ to simplify the notation. With the definition of $G(s)$ in (16) and $H(s)$ in (17), the CLTF $T(s)$, from the reference input $F_{\text{ex}}(s)$ to the output $V(s)$, is

$$T(s) = \frac{G(s)}{1 + G(s)H(s)} = \frac{1}{2B_r^\omega} \tag{18}$$

where B_r^ω is real and even. As expected, from a classical theoretical framework, the ACC controller achieves the well-known optimal velocity profile [13], expressed as

$$V(s) = T(s)F_{\text{ex}}(s) = \frac{F_{\text{ex}}(s)}{2B_r^\omega}. \tag{19}$$

Since the controller (17) is based on a simplified model of the real process, the sensitivity of the CLTF $T(s)$ in (18) to the variations in the open-loop transfer function $G(s)$ in (16) is of paramount importance for the performance analysis of the ACC loop under realistic conditions. The classical definition of the *sensitivity function* $S_G^T(s)$ provides a measure of how sensitive the CLTF $T(s)$ is to small variations in $G(s)$, namely,

$$S_G^T(s) = \frac{dT(s)}{dG(s)}\frac{G(s)}{T(s)} = \frac{1}{1 + G(s)H(s)}. \tag{20}$$

If $\left|S_G^T(s)\right| < 1$, the percentage change in $T(s)$ is less than the percentage change in $G(s)$, indicating a sensitivity improvement. Considering (20), and using (16) and (17), the sensitivity function for the ACC loop is given by

$$S_G^T(s) = \frac{(M + M_a^\omega)s^2 + B_r^\omega s + k}{2B_r^\omega s}. \tag{21}$$

Fig. 5 depicts $\left|S_G^T(\omega)\right|$, for the example, cylindrical WEC. It is straightforward to note that the ACC structure is extremely sensitive to the variations in $G(s)$, with $\left|S_G^T(\omega)\right|$ increasing dramatically for frequencies distant from the resonant frequency of the device $\omega_r \approx k/(M + m_\infty)^{1/2} \approx 0.67$ rads/s, where $\left|S_G^T(\omega)\right| = 0.5$.

Since the transfer function $G(s)$ is a function of the frequency-dependent added-mass M_a^ω and radiation damping B_r^ω (and both the frequency-independent mass of the device M and the hydrostatic stiffness k), it is useful to develop explicit expressions for the sensitivity of the closed-loop transfer function $T(s)$ to each hydrodynamic parameter separately.

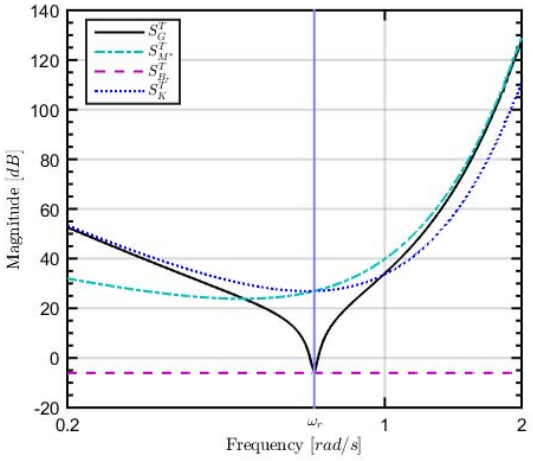

Fig. 5. Sensitivity functions for the ACC control loop. Blue vertical line: approximate resonant frequency $\omega_r = k/(M+m_\infty)^{1/2}$.

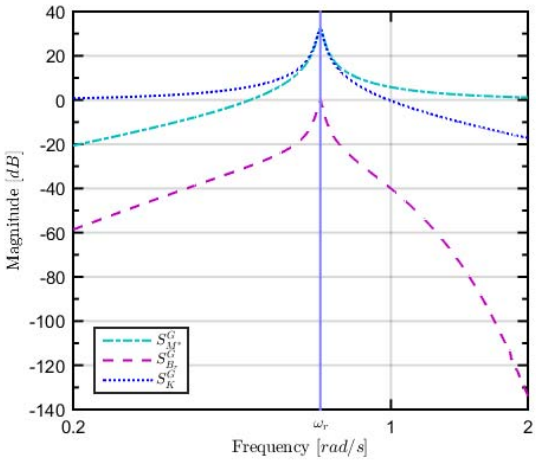

Fig. 6. Individual sensitivity of the open-loop transfer function $G(s)$ to each parameter. Blue vertical line: approximate resonant frequency $\omega_r = k/(M+m_\infty)^{1/2}$.

The general definition for the sensitivity of $T(s)$, to a specific parameter α, is given by

$$S_\alpha^T(s) = \frac{\alpha}{T(s)}\frac{dT(s)}{d\alpha} = S_G^T(s)S_\alpha^G(s) \tag{22}$$

where $S_\alpha^G(s)$ denotes the sensitivity of the open-loop transfer function $G(s)$ to the variations in the parameter α. Defining $M^* = M + M_a^\omega$, the sensitivity of $G(s)$, to each parameter M^*, B_r^ω, and k, can be independently evaluated as

$$S_{M^*}^G(s) = -\frac{M^*s^2}{M^*s^2 + B_r^\omega s + k} \tag{23}$$

$$S_{B_r}^G(s) = -\frac{B_r^\omega s}{M^*s^2 + B_r^\omega s + k} \tag{24}$$

$$S_k^G(s) = -\frac{k}{M^*s^2 + B_r^\omega s + k}. \tag{25}$$

When analyzing (23)–(25), it is possible to conclude that the open-loop transfer function is mainly sensitive to the variations in M^* at high frequency while, at low frequency, the sensitivity magnitude increases with the changes in the parameter k. In fact, this can be analytically illustrated as follows:

$$\lim_{s\to 0} S_{M^*}^G(s) = -\frac{1}{k} \approx 0 \quad \lim_{s\to\infty} S_{M^*}^G(s) = -1 \tag{26}$$

$$\lim_{s\to 0} S_k^G(s) = -1 \qquad \lim_{s\to\infty} S_k^G(s) = 0. \tag{27}$$

Fig. 6 illustrates the magnitude of each sensitivity function (23)–(25) for our cylindrical WEC example. It can be readily seen that the supremum for the three sensitivity functions occurs approximately at the resonant frequency of the device ω_r. In the case of $S_{B_r}^G(s)$, it is possible to conclude that the open-loop transfer function is only significantly affected near ω_r, i.e., $\left|S_{B_r}^G(j\omega_r)\right| = 1$.

From the traditional "tracking" control perspective, the controller $H(s)$ should be designed such that $S_G^T(s)$ reduces the open-loop sensitivity to parameter variations (at least in the input frequency range). However, in the ACC case, S_G^T dramatically *amplifies* the sensitivities defined in (23)–(25) at almost every frequency, except near ω_r, where the sensitivity magnitude is reduced (maximally) by a factor of two. Finally, considering (21), (23)–(25), the sensitivity of the CLTF $T(s)$, to the variations in M^*, B_r^ω and k, can be evaluated as

$$S_{M^*}^T(s) = S_G^T(s)S_{M^*}^G(s) = -\frac{M^*s^2}{2}B_r^\omega \tag{28}$$

$$S_{B_r}^T(s) = S_G^T(s)S_{B_r}^G(s) = -\frac{1}{2} \tag{29}$$

$$S_K^T(s) = S_G^T(s)S_K^G(s) = -\frac{k}{2B_r^\omega s}. \tag{30}$$

The three sensitivities defined in (28)–(30) are plotted in Fig. 5, along with the sensitivity function $S_G^T(s)$. Note that the following expression holds:

$$\left|S_{M^*}^T(s) + S_{B_r}^T(s) + S_K^T(s)\right| = \left|S_G^T(s)\right|. \tag{31}$$

From (28)–(30), and the frequency response plots of each sensitivity shown in Fig. 5, we note that the CLTF is particularly sensitive to M^* at high frequencies, while, for low frequencies, $T(s)$ is mainly sensitive to k, as expected from Fig. 6.

A further noteworthy observation is that the sensitivity of the CLTF to the variations in the radiation damping, i.e., $S_{B_r}^T(s)$, is frequency independent. In fact, from (29), we can deduce that $S_{B_r}^G(s) = -1/(2S_G^T(s))$.

In the following, and to provide an explicit analysis of the variation in the CLTF to specific structured uncertainties, it is assumed that the nominal transfer function $G(s)$ is affected by a *multiplicative modeling error* (MME), represented by a stable transfer function $G_\Delta(s)$, i.e., $\tilde{G}(s) = G(s)(1+G_\Delta(s))$, where $\tilde{G}(s)$ is the perturbed open-loop transfer function. These structured uncertainties are introduced by deviations in the system parameters, that is,

$$\tilde{G}(s) = \frac{s}{M^*(1+\delta M^*)s^2 + B_r^\omega(1+\delta B_r^\omega)s + k(1+\delta k)} \tag{32}$$

where $\{\delta M^*, \delta B_r^\omega, \delta k\} \subset [0, 0.2]$, which represents a maximum 20% deviation from the nominal value of each hydrodynamic parameter. To isolate the effect of each parameter

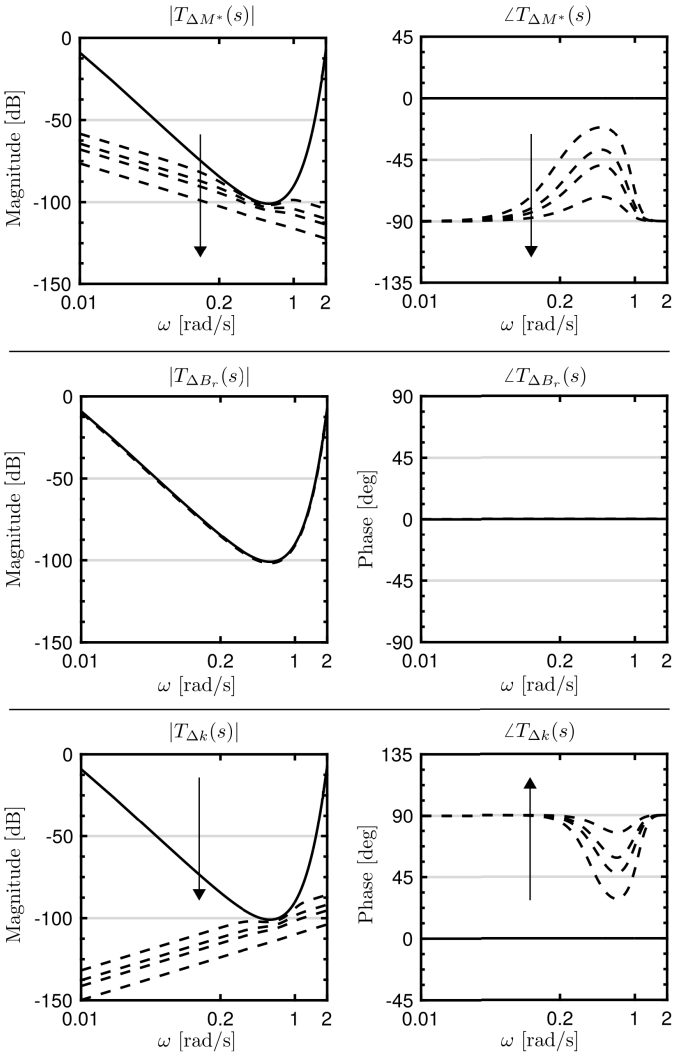

Fig. 7. Frequency response of each perturbed CLTF for the ACC loop, as defined in (33). The solid line depicts the nominal $T(s)$, whereas the dashed lines show the perturbed transfer functions, described in (33). Arrow: direction of increasing perturbation. Note that $\{\delta M^*, \delta B_r^\omega, \delta k\} \subset [0, 0.2]$.

deviation, the following *perturbed* CLTFs are defined:

$$\begin{aligned}
&\text{If } \tilde{G}(s)\Big|_{\delta B_r^\omega=\delta k=0,\delta M^*\neq 0} \text{ then } \tilde{T}(s) = T_{\Delta M^*}(s)\\
&\text{If } \tilde{G}(s)\Big|_{\delta M^*=\delta k=0,\delta B_r^\omega\neq 0} \text{ then } \tilde{T}(s) = T_{\Delta B_r}(s)\\
&\text{If } \tilde{G}(s)\Big|_{\delta M^*=\delta B_r^\omega=0,\delta k\neq 0} \text{ then } \tilde{T}(s) = T_{\Delta k}(s).
\end{aligned} \tag{33}$$

Fig. 7 depicts the frequency response of each perturbed transfer function defined in (33), for our example cylindrical WEC.

Consistent with the sensitivity function calculations in (28)–(30), Fig. 7 shows that the CLTF $T(s)$ is strongly affected by a deviation of the parameter M^* at high input frequencies while, at low frequencies, the uncertainty on the hydrodynamic parameter k causes a major deviation from the nominal profile. Nevertheless, even with a maximum deviation of 20% of B_r^ω from its nominal value, the frequency response of $T(s)$ remains almost unaffected, both in magnitude and phase.

B. AVT Structure

The AVT controller follows into a more traditional feedforward/feedback structure, which is straightforward to analyze. In particular, $S_{K_1}^T(s) = 1$, suggesting that the optimal velocity reference is uniformly sensitive to the errors in the calculation of K_1, or whatever other calculation is performed (see [23]) to evaluate the optimal velocity profile. Clearly, some compromise may be achieved so that a "desensitized" velocity profile might be calculated (see [10]) but while this might have positive implications for sensitivity, it is likely to negatively impact performance, to a greater or lesser extent.

However, the velocity tracking loop, controlled by K_2, is a classical feedback tracking loop and robust control techniques from the broad control systems science area can be liberally applied. A number of examples have been demonstrated in the literature, including an internal model controller (IMC), robustified using small gain and/or passivity [10], backstepping [28], and sliding mode control [11].

IV. Power Capture Sensitivity

In this section, the impact of modeling errors on power absorption is studied for the ACC and AVT control configurations. The WEC frequency-domain dynamical equation, including the control force F_{PTO}, is

$$Z_i(\omega)V(\omega) = F_{\text{ex}}(\omega) + F_{\text{PTO}}(\omega). \tag{34}$$

The average absorbed power is

$$P(V) = -\frac{1}{2}\Re\{V^* F_{\text{PTO}}\} = -\frac{1}{2}\Re(V^*(Z_i V - F_{\text{ex}})) \tag{35}$$

where the frequency dependence is omitted in order to lighten the notation. From (9) and/or (10), under maximum power transfer conditions, the optimal quantities are

$$\begin{cases}
V^o &= \dfrac{F_{\text{ex}}}{Z_i + Z_i^*} = \dfrac{F_{\text{ex}}}{2\Re\{Z_i\}}\\
F_{\text{PTO}}^o &= -\dfrac{Z_i^* F_{\text{ex}}}{Z_i + Z_i^*}\\
P^o &= \dfrac{1}{2}\Re\{Z_i\}\dfrac{|F_{\text{ex}}|^2}{(Z_i + Z_i^*)^2} = \dfrac{1}{8}\dfrac{|F_{\text{ex}}|^2}{\Re\{Z_i\}}.
\end{cases} \tag{36}$$

In the following, we consider that the optimal trajectory $\tilde{V}^o$, control force $\tilde{F}_{\text{PTO}}^o$, and average power $\tilde{P}^o$ are determined based on an inaccurate model of the system, represented as $\{\tilde{Z}_i, \tilde{F}_{\text{ex}}\} = \{Z_i + \epsilon_Z, F_{\text{ex}} + \epsilon_E\}$, ϵ_Z and ϵ_E being complex modeling errors.

A. ACC Structure

The ACC controller computes the optimal control law $\tilde{H}^o(\omega)$ based on the model $\{\tilde{Z}_i, \tilde{F}_{\text{ex}}\}$. The control law $\tilde{H}^o = \tilde{Z}_i{}^*$ is translated into the time domain as a linear operator (11).

The actual equation of motion, followed by the controlled WEC, is given as

$$Z_{\text{iV}} = F_{ex} - \tilde{H}^o V. \tag{37}$$

Replacing $\tilde{H}^o$ in (37) with $\tilde{Z}_i{}^*$ yields

$$(Z_i + \tilde{Z}_i^*)V = F_{\text{ex}}. \tag{38}$$

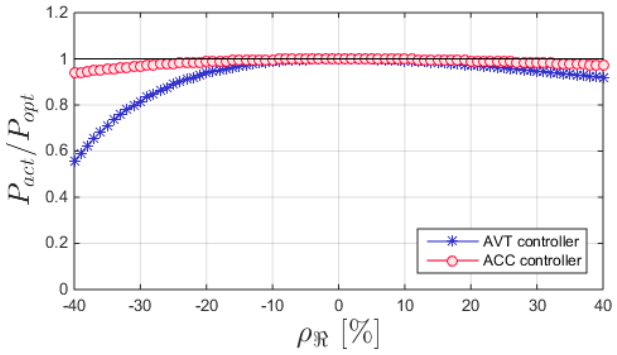

Fig. 8. Sensitivity of power absorption to relative errors on the radiation damping term.

The actual absorbed power is

$$P_{\text{act}} = -\frac{1}{2}\Re\left\{\frac{-|F_{\text{ex}}|^2\tilde{Z}_i^*}{|\tilde{Z}_i + Z_i^*|^2}\right\}. \tag{39}$$

Following some manipulation, P_{act} can be expressed as

$$P_{\text{act}} = P^o \frac{1+\rho_{\Re}}{1+\rho_{\Re}+\frac{1}{4}\rho_{\Re}^2+\frac{1}{4}\frac{\Im\{Z_i\}^2}{\Re\{Z_i\}^2}\rho_{\Im}^2} \tag{40}$$

where $\rho_{\Re} := \Re\{\epsilon_Z\}/\Re\{Z_i\}$ is the relative error in the radiation damping term, whereas $\rho_{\Im} = \Im\{\epsilon_Z\}/\Im\{Z_i\}$ represents the relative errors in either inertial or stiffness terms.

We can now analyze the sensitivity, P_{act}/P^o, to different error types. With modeling errors on damping terms only (i.e., errors in $\Re\{Z_i\}$), (40) yields

$$S_{\Re}(\rho_{\Re}) = \frac{1+\rho_{\Re}}{1+\rho_{\Re}+\frac{1}{4}\rho_{\Re}^2} \tag{41}$$

which is represented in Fig. 8. For $\rho_{\Re} \ll 1$, developing (41) up to order 2 yields $S_{\Re}(\rho_{\Re}) \approx 1 - 1/4\rho_{\Re}^2$. Therefore, $S_{\Re}(\rho_{\Re})$ depends quadratically on the relative error in the damping terms. For example, a 10% underestimation or overestimation of the radiation damping terms only reduces power absorption by approximately 0.25%.

Considering modeling errors in inertial or stiffness terms (i.e., errors in $\Im\{Z_i\}$), (40) yields

$$S_{\Im}(\rho_{\Im}) = \frac{1}{1+\frac{1}{4}\frac{\Im\{Z_i\}^2}{\Re\{Z_i\}^2}\rho_{\Im}^2}. \tag{42}$$

This time, the influence of modeling errors is weighted by a term, $1/4\Im\{Z\}^2/\Re\{Z\}^2$, which depends both on the specific WEC model and on the frequency considered, and which, for some frequencies, may be significantly greater than one. The power sensitivity to the errors in inertial or stiffness terms, for our example cylindrical WEC, is shown in Fig. 9 for varying frequency ω and error level $\rho_{\Im}$.

In particular, while $\Im\{Z\}$ takes large values at low frequency [due, in particular, to the k/ω^2 term in (7)], the damping terms in $\Re\{Z\}$ remain bounded and close to $B_r(0)$ and, therefore, $S_{\Im}(\rho_{\Im})$ is close to zero, even for small relative error levels.

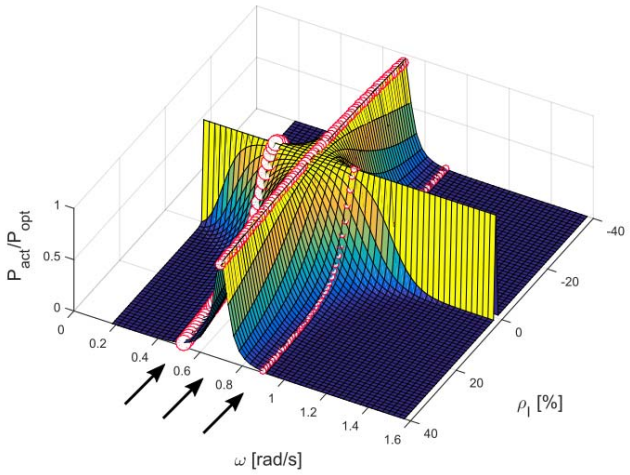

Fig. 9. Sensitivity of power absorption to inertial and stiffness term modeling errors in the ACC controller.

For 7-, 9-, and 12-s wave periods (equivalent to angular frequencies of 0.9, 0.7, and 0.52 rads/sec, respectively), the power sensitivity to errors in inertial or stiffness terms is highlighted in Fig. 9 and represented in Fig. 10 for comparison with the AVT case. It can be seen that the sensitivity is small for excitation periods in the neighborhood of the device resonant period ($T_{\text{res}} \approx 9$s), where the controller is redundant. In contrast, for excitation signal frequencies away from the resonant period, and where the controller is active, modeling errors have a large impact on power absorption. For example (see Fig. 10), with a wave period of 12 s, a relative error level of only 10% results in a 60% drop in the absorbed power, compared to the optimal (matched) control case.

As can be seen in Fig. 11, the absorbed power, with the ideal ACC controller, is not affected by errors in the excitation force. This is also confirmed by the absence of any terms involving F_{ex} in (40).

B. AVT Structure

In the AVT controller, the feedforward calculation (represented by K_1) computes the optimal velocity trajectory $\tilde{V}^o(\omega)$ based on the model $\{\tilde{Z}_i(\omega), \tilde{F}_{\text{ex}}(\omega)\}$. We assume that the velocity tracking loop follows $\tilde{v}^o(t)$ exactly.

Since the actual WEC behaves according to $\{Z_i, F_{\text{ex}}\}$ instead of $\{\tilde{Z}_i, \tilde{F}_{\text{ex}}\}$, the control force F^a_{PTO}, necessary to achieve $\tilde{V}^o$, differs from $\tilde{F}^o_{\text{PTO}}$, and is deduced from the dynamical equation

$$Z_i\tilde{V}^o = F_{\text{ex}} + F^a_{\text{PTO}}. \tag{43}$$

The actual average absorbed power is given as

$$P_{\text{act}} = -\frac{1}{2}\Re\{\tilde{V}^{o*}F^a_{\text{PTO}}\}. \tag{44}$$

Using (36) and (43) yields

$$P_{\text{act}} = -\frac{1}{2}\Re\left\{\frac{\tilde{F}_{\text{ex}}^*}{\tilde{Z}_i+\tilde{Z}_i^*}\left(\frac{Z_i\tilde{F}_{\text{ex}}}{\tilde{Z}_i+\tilde{Z}_i^*} - F_{\text{ex}}\right)\right\}. \tag{45}$$

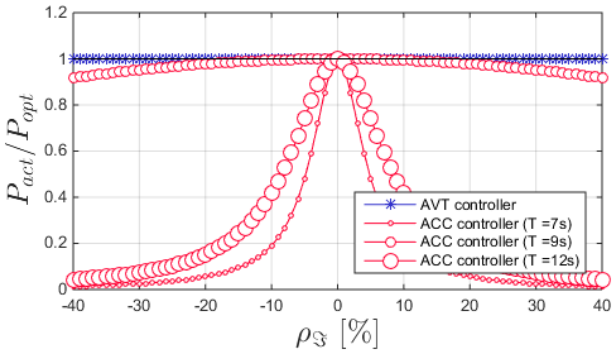

Fig. 10. Sensitivity of power absorption to inertial and stiffness errors in ACC and AVT controllers.

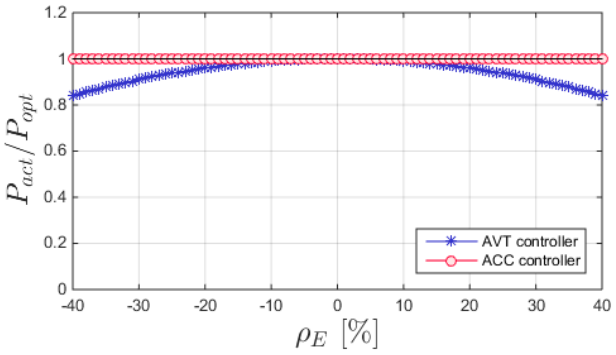

Fig. 11. Sensitivity of power absorption to excitation force modeling errors.

Following some further manipulation, P_{act} can be expressed as

$$P_{\text{act}} = P^o \frac{1 - |\rho_E|^2 + 2\rho_{\Re}(1 + \Re\{\rho_E\})}{(1 + \rho_{\Re})^2} \tag{46}$$

where $\rho_E := \epsilon_E / F_{\text{ex}}$ is the relative error in the excitation force term.

It is now straightforward to analyze the sensitivity of the extracted power to damping and excitation force modeling inaccuracies separately. From (46), when only damping term errors are present, it is possible to define a sensitivity function

$$S_{\Re}(\rho_{\Re}) : = \frac{P_{\text{act}}}{P^o} = \frac{1 + 2\rho_{\Re}}{(1 + \rho_{\Re})^2}. \tag{47}$$

The function $S_{\Re}(\rho_{\Re})$ is clearly frequency independent and is plotted in Fig. 8. Two noteworthy observations may be derived from (47) and Fig. 8 in the following.

1) Assuming $\rho_{\Re} \ll 1$, and developing (47) up to order 2, yields $S_{\Re}(\rho_{\Re}) \approx 1 - \rho_{\Re}^2$. Therefore, for small errors in radiation damping, the loss in power production evolves quadratically with the relative error: A 10% overestimation or underestimation of damping terms results in a loss of approximately 1% in power extraction.
2) Considered over a wider range of error values, the sensitivity function in (47) is not symmetric with respect to the sign of the error. More precisely, overestimation of the radiation damping terms has a relatively small impact on power production, compared to underestimation of the same magnitude, also confirmed by the simulation results in [29]. For example, overestimating the damping coefficient by 40% results in a power loss of less than 10%. This suggests that the damping term included in the controller should be overconservative rather than underconservative.

We can also note that power absorption, under AVT control, is insensitive to the modeling errors in inertial and stiffness terms, since (46) is independent of $\rho_{\Im}$, and so is uniformly equal to one shown in Fig. 10.

Finally, analyzing the sensitivity with respect to a relative error in excitation force yields

$$S_E(\rho_E) = 1 - |\rho_E|^2 \tag{48}$$

where $S_E(\rho_E)$ is quadratic and only depends on the magnitude of ρ_E. $S_E(\rho_E)$ is plotted in Fig. 11 for the case where ϵ_E and F_{ex} have the same phase in $[0; \pi]$, i.e., ρ_E takes positive and negative real values. If the error magnitude represents 10 % of the excitation force magnitude, the power extraction decreases by only 1%.

V. Simulation Results

For the numerical results presented in this section, the WEC model considered is a heaving cylinder with 7 [m] radius, 20 [m] height, and 16 [m] draft, with the hydrodynamic parameters $[M_a(\omega), B_r(\omega), H_{\text{ex}}(\omega)]$ calculated using the WAMIT utility.

A. Control Implementation

1) AVT Control Loop: The AVT controller shown in Fig. 4 is based on the procedure proposed in [10]. In particular, the velocity setpoint calculation is based on a frequency-dependent proportional law, $K_1(s) = 1/2\,(B(\omega_0))$, where the central frequency ω_0 is adapted in real time, based on the peak frequency of the excitation force, estimated with an extended Kalman filter (EKF). The nominal feedback controller, $K_2(s)$, is based on the IMC procedure, as described in [10].

Two variants of the AVT controller shown in Fig. 4 are implemented.

1) In the first one, simply termed *AVT*, the tracking feedback controller, $K_2(s)$, is based on the nominal model of the WEC. Therefore, any modeling error has an impact on both the reference velocity generation *and* on the tracking loop.
2) In the *robust AVT*, $K_2(s)$ is based on a positive definite approximation of the nominal feedback controller, following the method proposed in [10]. Therefore, good tracking can be achieved in spite of modeling errors (though the velocity setpoint itself may be affected by modeling errors). The robust AVT is closer to the idealized situation described in Section IV-B.

2) ACC Control Loop: The feedback law of the ACC controller shown in Fig. 3, $H(s)$, is designed based on the reciprocal of the complex conjugate of a second-order approximation of the nominal plant [30]

$$H(s) = F(s)/G_{\text{eq}}^*(s). \tag{49}$$

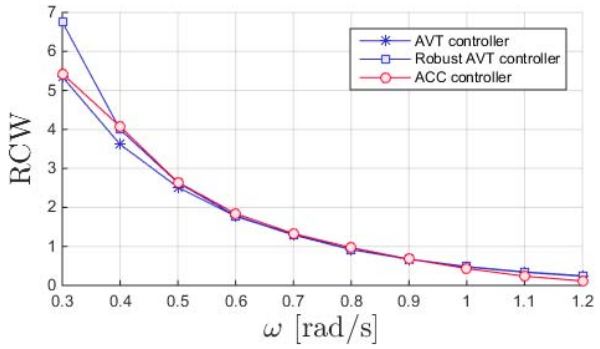

Fig. 12. Simulation results: RCW for AVT, robust AVT, and ACC controllers under nominal conditions. ω: peak wave frequency in the Ochi spectral model.

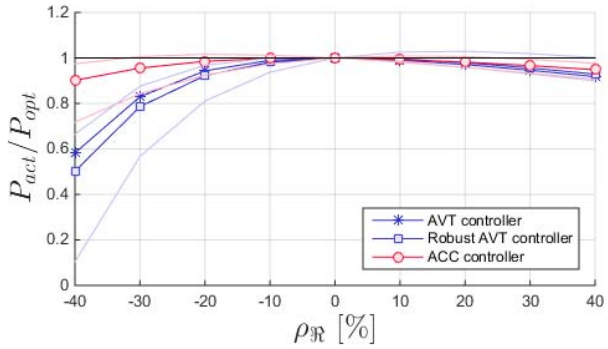

Fig. 13. Simulation results: sensitivity of power absorption to damping term modeling errors. Sensitivity values are averaged over the range of wave conditions. For the robust AVT (respectively ACC) controller, the minimum and maximum sensitivity values across all wave conditions are indicated by means of blue thin (respectively red) lines.

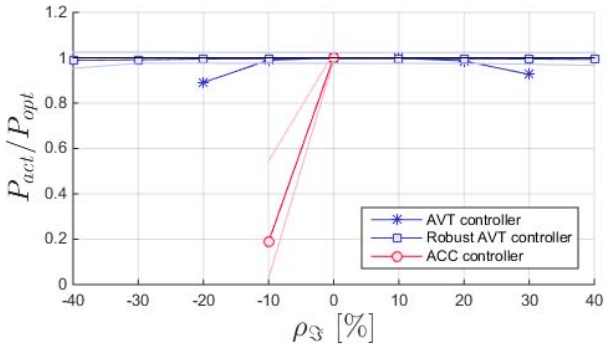

Fig. 14. Simulation results: sensitivity of power absorption to inertial term modeling errors. Missing points indicate the cases where the simulation is unstable. Sensitivity values are averaged over the range of wave conditions. For the robust AVT (respectively ACC) controller, the minimum and maximum sensitivity values across all wave conditions are indicated by means of blue thin (respectively red) lines.

An additional bandpass filter $F(s)$ is needed in order to make the controller realizable, $F(s) = 100s/[(s + 0.002) \cdot (s + 100)]$, with a negligible effect on the system over the typical frequency range of incident waves.

The controller $H(s)$ cannot be effectively approximated with a positive real function due to the stringent specification in (49). Therefore, a robust control, based on passivity, cannot be designed as for the AVT case.

For brevity, motion constraints are not considered in this paper, but it can be noted that, while the AVT structure offers a natural framework for incorporating both motion and force constraints (see [10] or [23]), the ACC structure does not lend itself well to constraint handling.

B. Numerical Setup

Numerical simulations were setup in MATLAB Simulink[1]. The simulations were driven by an excitation force signal computed from (2), with a stochastic wave elevation signal $\eta(t)$ generated from single-peak Ochi spectra with various peak frequencies, and with a significant wave height of $H_s = 1$ [m] and $\lambda = 3$, based on the procedure in [31]. The excitation force was assumed known throughout the simulations.

C. Simulation Results

1) Under Nominal Conditions: In the absence of modeling errors, AVT, robust AVT, and ACC controllers achieve a very similar relative capture width (RCW) [32] (see Fig. 12), reflecting the fact that both AVT and ACC are largely based on (9). The agreement between the three controllers is almost perfect in the most typical wave conditions, i.e., for peak periods in the range of 5–15 [s] (corresponding to $\omega = 0.4 - 1$ [rad/s]).

2) Errors in Radiation Damping Terms: As in the theoretical calculations, the power absorption sensitivity is calculated as P_{act}/P^o and is shown in Fig. 13 for different levels of damping term modeling errors. For readability, the results are averaged over the complete range of peak wave frequencies shown in Fig. 12 (but are relatively insensitive to frequency). We can note that in the following.

1) For the AVT loop, the sensitivity of power absorption to damping term errors shows the same order of magnitude as predicted by theory (Fig. 8), and the same asymmetry with respect to the sign of the error; overestimation of the damping term does not significantly affect power production, compared to underestimation. This is true for both the simple AVT and robust AVT loops.
2) The ACC loop shows a lower sensitivity than AVT to damping errors as was also the case shown in Fig. 8.

3) Errors in Inertial Terms: Fig. 14 shows the sensitivity of power absorption to modeling errors in the inertial terms. The results are averaged over the range of peak wave frequencies shown in Fig. 12. Notably,

1) For the simple AVT loop, small errors in the inertial terms have little or no impact on power absorption; however, beyond a 20–30% error level, tracking cannot be carried out successfully, and the velocity tracking loop becomes unstable. However, with the robust AVT approach, the trajectory is successfully tracked in spite of the modeling errors. As a result, there is virtually no sensitivity of power absorption to the inertial term

[1]https://U.K..mathworks.com/products/simulink.html

modeling errors, as was predicted from theoretical calculations (Fig. 10).

2) For the ACC loop, the sensitivity properties are worse than predicted by the theoretical calculations (Figs. 10 and 9); even small modeling errors have the potential to make the control loop unstable. We note that, in the theoretical power calculations, instability issues are not considered (only power performance, assuming stable tracking).

VI. Conclusion

Though both ACC and AVT ostensibly chase the same impedance matching objective, this paper demonstrates that the controllers show significantly different sensitivities/robustness to real hydrodynamic modeling errors. In WEC device modeling, there are a variety of reasons that the models will inevitably contain errors, as discussed in Section I. Therefore, the *actual* performance of a WEC controller, under realistic conditions, is highly dependent on its sensitivity properties.

Some generic results, from Section II-C, are noteworthy. Accurate modeling of velocity-dependent terms (radiation damping, drag, and so on) is important while, under unconstrained conditions (or just position and velocity constraints), for the AVT controller, there is insensitivity to inertial and stiffness terms. Under PTO force constraints, the AVT controller may be sensitive to inertial and stiffness term errors (greater sensitivity under more severe constraints), while the velocity tracking loop can be robustified to these sensitivities. With regard to damping term errors, Section IV highlights the need to overestimate rather than underestimate, velocity-dependent damping. This has important implications for the use of linear hydrodynamic models, where viscous damping effects are frequently ignored completely.

While the CLTF sensitivity for the ACC controller, presented in Fig. 5, would cause great alarm to a practicing feedback control engineer, with values of over $+100$ [dB] away from resonance, the sensitivity of power production (arguably a more important quantity in wave energy systems) is somewhat less dramatic. Nevertheless, there is significant power loss in the ACC controller due to inertial and stiffness errors (shown in Fig. 10), especially compared to the AVT controller. For the AVT controller, there is a potential vulnerability in the feedforward calculation of the optimal velocity profile, but thereafter, standard robust control techniques can be applied to the velocity-following loop. Overall, the AVT loop presents better performance than ACC under realistic conditions, highlighted by the simulation results in Section V. However, it needs to be borne in mind that, unlike the ACC controller, the AVT controller also requires estimation and forecasting of future $f_{\mathrm{ex}}(t)$ which, though eminently achievable, will inevitably introduce some approximation errors, as documented in [26].

References

[1] U. A. Korde and J. V. Ringwood, *Hydrodynamic Control of Wave Energy Devices*. Cambridge, U.K.: Cambridge Univ. Press, 2016.

[2] K. Budal and J. Falnes, "Interacting point absorbers with controlled motion," in *Power From Sea Waves*. New York, NY, USA: Academic, 1980, pp. 381–399.

[3] A. Clément and A. Babarit, "Discrete control of resonant wave energy devices," *Philos. Trans. Roy. Soc. A, Math. Phys. Eng. Sci.*, vol. 370, no. 1959, pp. 288–314, 2012.

[4] J. Hals, J. Falnes, and T. Moan, "Constrained optimal control of a heaving buoy wave-energy converter," *J. Offshore Mech. Arctic Eng.*, vol. 133, no. 1, 2011, Art. no. 011401.

[5] J. V. Ringwood, G. Bacelli, and F. Fusco, "Energy-maximizing control of wave-energy converters: The development of control system technology to optimize their operation," *IEEE Control Syst.*, vol. 34, no. 5, pp. 30–55, Oct. 2014.

[6] M. Penalba and J. V. Ringwood, "A review of wave-to-wire models for wave energy converters," *Energies*, vol. 9, no. 7, p. 506, 2016.

[7] K. Zhou and J. C. Doyle, *Essentials of Robust Control*, vol. 104. Upper Saddle River, NJ, USA: Prentice-Hall 1998,

[8] D. Valério, P. Beirão, M. J. G. C. Mendes, and J. S. D. Costa, "Robustness assessment of model-based control for the archimedes wave swing," in *Proc. Eur. Control Conf. (ECC)*, Aug. 2009, pp. 3749–3754.

[9] A. O'Sullivan and G. Lightbody, "Power maximisation of a wave energy converter using predictive control: Robustness to system mismatch," in *Proc. 12th Eur. Wave Tidal Energy Conf. (EWTEC)*, Aug. 2017, p. 10121.

[10] F. Fusco and J. V. Ringwood, "Hierarchical robust control of oscillating wave energy converters with uncertain dynamics," *IEEE Trans. Sustain. Energy*, vol. 5, no. 3, pp. 958–966, Jul. 2014.

[11] A. Wahyudie, M. A. Jama, O. Saeed, H. Noura, A. Assi, and K. Harib, "Robust and low computational cost controller for improving captured power in heaving wave energy converters," *Renew. Energy*, vol. 82, pp. 114–124, Oct. 2015.

[12] M. Green and D. J. Limebeer, *Linear Robust Control*. North Chelmsford, MA, USA: Courier Corp., 2012.

[13] J. Falnes, *Ocean Waves and Oscillating Systems: Linear Interactions Including Wave-Energy Extraction*. Cambridge, U.K.: Cambridge Univ. Press, 2002.

[14] W. Cummins, "The impulse response function and ship motions," *Schiffstechnik*, vol. 9, pp. 101–109, Oct. 1962.

[15] G. Giorgi and J. V. Ringwood, "Nonlinear Froude-Krylov and viscous drag representations for wave energy converters in the computation/fidelity continuum," *Ocean Eng.*, vol. 141, pp. 164–175, Sep. 2017.

[16] T. Perez and T. I. Fossen, "Practical aspects of frequency-domain identification of dynamic models of marine structures from hydrodynamic data," *Ocean Eng.*, vol. 38, nos. 2–3, pp. 426–435, 2011.

[17] N. Faedo, Y. Peña-Sanchez, and J. V. Ringwood, "Finite-order hydrodynamic model determination for wave energy applications using moment-matching," *Ocean Eng.*, vol. 163, pp. 251–263, Sep. 2018.

[18] G. Giorgi, M. R. Penalba, and J. Ringwood, "Nonlinear hydrodynamic models for heaving buoy wave energy converters," in *Proc. Asian Wave Tidal Energy Conf. (AWTEC)*, Singapore, 2016, pp. 1–10.

[19] J. Hals, J. Falnes, and T. Moan, "A comparison of selected strategies for adaptive control of wave energy converters," *J. Offshore Mech. Arctic Eng.*, vol. 133, no. 3, pp. 031101–031113, 2011.

[20] C. H. Lee and J. N. Newman, "WAMIT user manual, versions 6.3, 6.3PC, 6.3S, 6.3S-PC," WAMIT, Chestnut Hill, MA, USA, Tech. Rep., 2006.

[21] R. Hansen, "Design and control of the powertake-off system for a wave energy converter with multiple absorbers," Ph.D. dissertation, Dept. Energy Technol., Aalborg Univ., Aalborg, Denmark, 2013.

[22] S. R. K. Nielsen, Q. Zhou, M. M. Kramer, B. Basu, and Z. Zhang, "Optimal control of nonlinear wave energy point converters," *Ocean Eng.*, vol. 72, pp. 176–187, Nov. 2013.

[23] N. Faedo, S. Olaya, and J. V. Ringwood, "Optimal control, MPC and MPC-like algorithms for wave energy systems: An overview," *IFAC J. Syst. Control*, vol. 1, pp. 37–56, Sep. 2017.

[24] F. Fusco and J. V. Ringwood, "Short-term wave forecasting for real-time control of wave energy converters," *IEEE Trans. Sustain. Energy*, vol. 1, no. 2, pp. 99–106, Jul. 2010.

[25] Y. Peña-Sanchez, A. Mérigaud, and J. V. Ringwood, "Short-term forecasting of sea surface elevation for wave energy applications: The autoregressive model revisited," *IEEE J. Ocean. Eng.*, to be published.

[26] F. Fusco and J. V. Ringwood, "A model for the sensitivity of non-causal control of wave energy converters to wave excitation force prediction errors," in *Proc. CD-ROM*, Southampton, 2011.

[27] A. Mérigaud and J. V. Ringwood, "Optimal trajectories, nonlinear models and constraints in wave energy device control," in *Proc. IFAC World Congr.*, Toulouse, France, 2017, pp. 16215–16220.
[28] R. Genest and J. V. Ringwood, "Receding horizon pseudospectral control for energy maximization with application to wave energy devices," *IEEE Trans. Control Syst. Technol.*, vol. 25, no. 1, pp. 29–38, Jan. 2017.
[29] A. C. M. O'Sullivan and G. Lightbody, "The effect of viscosity on the maximisation of electrical power from a wave energy converter under predictive control," *IFAC-PapersOnLine*, vol. 50, no. 1, pp. 14698–14704, 2017.
[30] F. Fusco and J. Ringwood, "Suboptimal causal reactive control of wave energy converters using a second order system model," in *Proc. 21st Int. Offshore Polar Eng. Conf.*, 2011, pp. 687–694.
[31] J. Figwer, "A new method of random time-series simulation," *Simul. Pract. Theory*, vol. 5, no. 3, pp. 217–234, 1997.
[32] A. Babarit, "A database of capture width ratio of wave energy converters," *Renew. Energy*, vol. 80, pp. 610–628, Aug. 2015.

John V. Ringwood (SM'97) received the Diploma degree in electrical engineering from the Dublin Institute of Technology, Dublin, Ireland, and the Ph.D. degree in control systems from Strathclyde University, Glasgow, Scotland, in 1981 and 1985, respectively.

He is currently a Professor of electronic engineering from Maynooth University, Co. Kildare, Ireland, where he is also the Director of the Centre for Ocean Energy Research. His current research interests include cover time series modeling, wave energy, control of plasma processes, and biomedical engineering.

Dr. Ringwood is a Chartered Engineer and a fellow of Engineers Ireland.

Alexis Mérigaud received the Engineering Diploma degree in engineering (energy management and economics) from ENSTA ParisTech, Paris, France, the Ph.D. degree from the Centre for Ocean Energy Research (COER), Maynooth University, Ireland, in 2019, and the master's degree in public administration with Sciences Po, Paris, France.

He was experienced in energy including economic modeling, as well as technical regulatory aspects, of energy networks and markets. He is currently an Engineer with IFP Energies Nouvelles, Rueil-Malmaison, France, where he is involved in the control of wave energy systems.

Nicolás Faedo received the Degree in automation and control engineering from the National University of Quilmes, Buenos Aires, Argentina, in 2015. He is currently pursuing the Ph.D. degree in nonlinear control of wave energy devices with the Centre for Ocean Energy Research Maynooth University, Co Kildare, Ireland.

He was involved in model identification and optimization of cold rolling processes with the bachelor's scholarship. In 2016, he was involved in the control of complex networks, particularly related to synchronization control of coupled chaotic nonlinear oscillators, with specific biomedical applications.

Francesco Fusco received the master's degree in industrial automation engineering from Università Politecnica delle Marche (UNIVPM), Ancona, Italy, in 2008, and the Ph.D. degree in electronic engineering from the National University of Ireland (NUI), Maynooth, Ireland, in 2012.

Since 2012, he has been a Research Scientist with the Smarter Cities Technology Centre, IBM Research—Ireland, Dublin, Ireland.

Dr. Fusco is a Chartered Engineer in Italy.